Energies and densities of electrons confined in elliptical and ellipsoidal quantum dots

Avik Halder[1,2] and Vitaly V. Kresin[2]

[1]*Materials Science Division*
Argonne National Laboratory, 9700 South Cass Avenue, Argonne, IL 60439, USA

[2]*Department of Physics and Astronomy*
University of Southern California, Los Angeles, CA 90404, USA

JULY 2016

SUBMITTED TO

Journal of Physics: Condensed Matter

IOP Publishing Journal of Physics: Condensed Matter
J. Phys.: Condens. Matter **00** (2016) 000000 (9pp) UNCORRECTED PROOF

Energies and densities of electrons confined in elliptical and ellipsoidal quantum dots

Avik Halder[1,2] **and Vitaly V Kresin**[2]

[1] Materials Science Division, Argonne National Laboratory, 9700 South Cass Avenue, Argonne, IL 60439, USA
[2] Department of Physics and Astronomy, University of Southern California, Los Angeles, CA 90404, USA

AQ1 E-mail: xxxx

Received 3 June 2016, revised 16 July 2016
Accepted for publication 20 July 2016
Published

Abstract

We consider a droplet of electrons confined within an external harmonic potential well of elliptical or ellipsoidal shape, a geometry commonly encountered in work with semiconductor quantum dots and other nanoscale or mesoscale structures. For droplet sizes exceeding the effective Bohr radius, the dominant contribution to average system parameters in the Thomas–Fermi approximation comes from the potential energy terms, which allows us to derive expressions describing the electron droplet's shape and dimensions, its density, total and capacitive energy, and chemical potential. The analytical results are in very good agreement with experimental data and numerical calculations, and make it possible to follow the dependence of the properties of the system on its parameters (the total number of electrons, the axial ratios and curvatures of the confinement potential, and the dielectric constant of the material). An interesting feature is that the eccentricity of the electron droplet is not the same as that of its confining potential well.

Keywords: quantum dots, nanoclusters, self-consistent field, Thomas–Fermi theory

AQ2 (Some figures may appear in colour only in the online journal)

1. Introduction

Advances in the field of nanotechnology have led to the development of nanoscale quantum dots (QD) in which electrons are spatially confined within dimensions ranging from just a few up to several hundreds of nanometers.

If the motion of the electrons is effectively restricted to a two-dimensional (2D) plane, as occurs, e.g. in semiconductor inversion layers, disks of electrons sandwiched within semiconductor pillars, and self-assembled islands within layered heterostructres [1, 2] then by adding a weaker in-plane confinement one obtains a 2D QD island. Restriction to two dimensions is achieved when there is strong transverse quantization, that is, when the layer thickness becomes commensurate with the effective Bohr radius,

$$a_{\mathrm{B}}^{*} = \frac{\hbar^2 \varepsilon}{m^* e^2}. \tag{1}$$

Here e and m^* are the electron charge and effective mass, and ε is the dielectric constant of the semiconductor material. For example, for InGaAs dots described in [1], the disk diameter is a few hundred nm, its thickness is about 10 nm, and $a_{\mathrm{B}}^{*} \approx 10$ nm [3].

In the lateral (soft) direction the 2D 'artificial atom' is confined within a potential well V created by external electrostatic gates and/or by the sidewalls, and this potential can frequently be approximated as quadratic. In this respect the QD artificial atoms differ from real atoms, in which the electron cloud resides within the Coulomb potential of the nucleus rather than within a parabolic bowl. Another important distinction

JNL:CM PIPS: AA3492 TYPE: PAP TS: NEWGEN DATE:27/7/16 EDITOR: IOP SPELLING: US

lies in the fact that the dot's potential does not need to be central: by a suitable design of the electrode or pillar shape, the confinement can be made asymmetric. An important case is when the potential is elliptical, i.e. with different oscillator curvatures along is two principal axes.

A 3D analog of the above corresponds to an electron cloud within a 3D harmonic oscillator potential. This can arise for QDs grown in semiconductor heterostructures [4] as well as for electrons confined to the interior of metal nanocluster particles [5, 6]. In the latter case the effective Bohr radius and consequently the QD dimension can be 1–2 orders of magnitude smaller than for semiconductors.

In analyzing the behavior of QD electrons, quantities of interest include the shape and depth of the mean field, the shape and size of the electron cloud, its total energy, the chemical potential, etc. Evaluating these quantities as a function of the number of electrons in the dot must be done in a self-consistent manner, accounting for the electron–electron interaction and screening. Of the large number of calculations in the literature the majority employ numerical methods such as exact diagonalization for few-electron dots, and Hartree–Fock, density-functional or related treatments for larger ones. Thus, identifying a reliable analytical approach is certainly worthwhile: it can enable one to map the system's behavior over a large parameter space and to track the interdependence between different parameters. This is the goal of the present paper.

In the study of finite Fermi systems it has been found convenient to separate two contributions to their ground-state properties. One is the average variation of the system's characteristics with the number of constituent particles (such as the liquid-drop model of nuclei or the Thomas–Fermi description of atoms or metal clusters), which can be referred to as the 'smooth' part; and the other is a superimposed structure of quantum oscillations. This is referred to as the 'shell-correction method' (see, e.g. [7, 8]). In the present context, the statistical approximation [9–13] is an accurate descriptive tool for the calculation of average parameters of finite systems, such as an electron droplet within a QD. What's more, it has been shown [14] that it rigorously reduces to the electrostatic limit when the QD dimension is sufficiently large; see section 2. As a result, it is possible to describe the properties of the dot electron cloud analytically even for non-centrally-symmetric confining potentials. This is done in sections 3 and 4 for 2D and 3D quantum dots, respectively, where we present expressions for the electron density distribution functions and their shapes, and for the electron energies, chemical potentials, and capacitive energies. The efficacy of the results is affirmed by comparisons with experimental data and numerical calculations from the literature. Section 5 contains a summary.

2. Semiclassical theory and its classical limit

As mentioned, it is well known that a many-electron system within a smooth potential well can be accurately described by the semiclassical statistical approach, namely the Thomas–Fermi (TF) theory. This treatment yields reliable values of physical quantities which are averaged over the quantum oscillations. The TF method is based on the picture that the maximum kinetic energy of the electron gas, treated semiclassically, cannot exceed the local depth of the self-consistent potential well (as measured relative to the chemical potential):

$$\frac{p_{\mathrm{F}}^2(\vec{r})}{2m^*} + V(\vec{r}) + e\varphi(\vec{r}) = \mu \tag{2}$$

Here p_{F} is the local value of the Fermi momentum, the chemical potential of the electron system is denoted by μ ($\mu = 0$ for a neutral isolated atom, but not in general), V is the external confining potential, and φ is the electrostatic potential generated by the electron cloud. The charge e is defined to be a negative quantity.

In 2D $p_{\mathrm{F}}^2 = 2\pi\hbar^2 n$ where n is the number of electrons per unit area. For electrons confined within a 3D dot $p_{\mathrm{F}}^2 = \hbar^2(3\pi^2 n)^{2/3}$ where n is the number of electrons per unit volume. An important observation [14] is that the relative magnitude of the ground state kinetic energy p_{F}^2 term, which derives from quantum effects, is proportional to the factor a_{B}^*/R where R is the radius of the dot's electron cloud. This means that for sufficiently extended systems (such as, e.g. the InGaAs dots mentioned above) where this factor is $\ll 1$, it can be sufficient to retain only the following from equation (2):

$$V(\vec{r}) + e\varphi(\vec{r}) = \mu, \tag{3}$$

which can be recognized as the classical equation of force equilibrium. The electrostatic potential is given by

$$\varphi(\vec{r}) = \frac{e}{\varepsilon}\int \frac{n(\vec{r}')}{|\vec{r} - \vec{r}'|} d^D\vec{r}' \tag{4}$$

with $D = 2$ or 3 for a 2D or 3D QD, respectively.

Quantum deviations from equation (3) show up only in the region near the dot edge, $r \sim R$, because here the density profile is changing rapidly and the kinetic energy term in the TF differential equation $\nabla^2 p_{\mathrm{F}}^2(\vec{r})/2m^* - 4\pi e n(\vec{r})/\varepsilon + \nabla^2 V(\vec{r}) = 0$ (obtained from equation (2) by differentiation) becomes large. Treatments of the full TF equation incorporating edge effects for such systems as axially symmetric 2D quantum dots, planar metallic surfaces, metal clusters and 3D parabolically confined electrons can be found, e.g. in [6, 15–18].

In the following, we make use of the classical limit to consider harmonically confined QD and to derive expressions for those parameters which are well represented by this formalism: the size and shape of the electron cloud and the energetics of the system. In particular, we focus on the case of elliptical (or ellipsoidal) dots, for which a full analytical solution of the TF equation is unavailable but a solution in the classical limit can be written out in closed form.

3. 2D elliptical quantum dots

3.1. Electron distribution

We consider an electron island within an elliptical external potential well

$$V(\vec{r}) = \gamma_x x^2 + \gamma_y y^2 \tag{5}$$

where γ_x and γ_y determine the parabolic curvature along the x and y axes, respectively. The zero of energy is set at the minimum of V for convenience. Sometimes it is also convenient to impose the constant area constraint $\gamma_x\gamma_y = \gamma^2$ by defining the deformation parameter δ via $\gamma_x = \delta^{-1/2}\gamma$, $\gamma_y = \delta^{1/2}\gamma$. In the present picture the external field is everywhere balanced by the electron–electron electrostatic repulsion. The local kinetic energy of the particles is neglected, and at every point the potential energy of the electron cloud satisfies equation (3).

We assume that the QD contains N electrons and that the electron density n vanishes outside the boundary of an ellipse with semi-major and semi-minor radii a and b, respectively. Note an important point: it should not be automatically assumed that the ellipse circumscribing the electron density has exactly the same shape as the confining potential V, equation (5). In fact, the calculation will show that it does not.

Combining equations (3)–(5), we have

$$e^{*2}\int_0^a\int_0^b \frac{n(x',y')}{|\vec{r}-\vec{r}'|}\mathrm{d}x'\mathrm{d}y' = \mu - \gamma_x x^2 - \gamma_y y^2, \tag{6}$$

where the effective charge is defined as $e^* \equiv e/\varepsilon^{1/2}$.

This 2D integral equation has a well-known solution which arises not only in the electrostatics of a flattened ellipsoid but also in the problem of an elastic elliptical contact (the Hertz contact problem) [19]. Previously, a similar approach has been employed to analyze electron 'dimple' islands on liquid helium surfaces [20, 21].

One finds that the electron number density inside the dot has the following form:

$$n(x,y) = n_0\sqrt{1 - \frac{x^2}{a^2} - \frac{y^2}{b^2}} \tag{7}$$

Here $\{a,b\}$ define the outer boundary of the electron cloud, as specified above, and the normalization condition $\int n(x,y)\mathrm{d}x\mathrm{d}y = N$ yields

$$n_0 = \frac{3N}{2\pi ab} \tag{8}$$

for the density at the center [20]. As mentioned above, near the very edge the solution (7) requires quantum correction as the proper density always has a decay tail rather than an abrupt drop.

The next step is to relate the shape of the electron cloud to that of its external confining potential by solving for the semi-axes $\{a,b\}$ in terms of $\{\mu,\gamma_x,\gamma_y\}$. For this we again refer to the electrostatic problem described, e.g. in [19] where the following identity is derived:

$$\begin{aligned}\int_0^a\int_0^b \frac{\sqrt{1 - x'^2/a^2 - y'^2/b^2}}{|\vec{r}-\vec{r}'|}\mathrm{d}x'\mathrm{d}y' \\ = \frac{1}{2}\pi ab\int_0^\infty \frac{1 - x^2/(a^2+\xi) - y^2/(b^2+\xi)}{\sqrt{\xi(a^2+\xi)(b^2+\xi)}}\mathrm{d}\xi\end{aligned} \tag{9}$$

Comparing this relation with equations (6)–(8), we can immediately identify

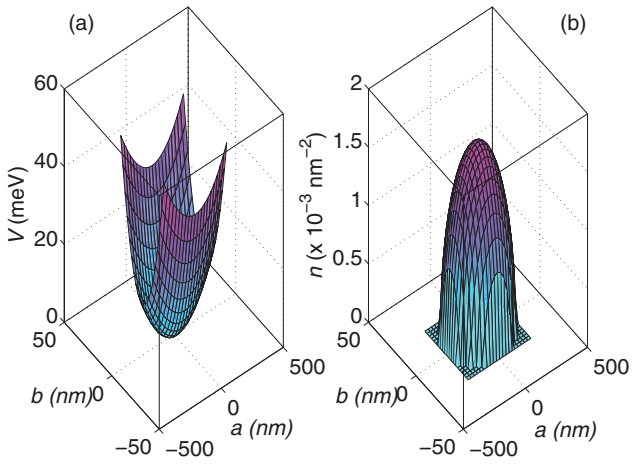

Figure 1. (a) An elliptical harmonic confining potential $V(x,y)$ with deformation parameter $\delta = \gamma_y/\gamma_x = 43$ and confinement force constant $\gamma = 3.8$ μeV nm^{-2}, as defined in equation (5) ff. (b) The corresponding electron number density distribution, equation (7), inside this asymmetric quantum dot for $N = 20$ and $\varepsilon = 12.9$, $m^* = 0.065$, which are the parameters [24] for $In_{0.05}Ga_{0.95}As$ samples in [3, 25].

$$\mu = \frac{3}{4}Ne^{*2}\int_0^\infty \frac{\mathrm{d}\xi}{\sqrt{\xi(a^2+\xi)(b^2+\xi)}} = \frac{3}{2}\frac{Ne^{*2}}{a}K(k), \tag{10}$$

$$\begin{aligned}\gamma_x &= \frac{3}{4}Ne^{*2}\int_0^\infty \frac{\mathrm{d}\xi}{(a^2+\xi)\sqrt{\xi(a^2+\xi)(b^2+\xi)}} \\ &= \frac{3}{2}\frac{Ne^{*2}}{a^3}\frac{K(k)-E(k)}{k^2},\end{aligned} \tag{11}$$

$$\begin{aligned}\gamma_y &= \frac{3}{4}Ne^{*2}\int_0^\infty \frac{\mathrm{d}\xi}{(b^2+\xi)\sqrt{\xi(a^2+\xi)(b^2+\xi)}} \\ &= \frac{3}{2}\frac{Ne^{*2}}{a^3}\frac{\frac{a^2}{b^2}E(k) - K(k)}{k^2}.\end{aligned} \tag{12}$$

Here [22] K and E are the complete elliptic integrals of the first and second kind [23][3] and $k = \sqrt{1 - b^2/a^2}$ is the eccentricity of the electron cloud's boundary ($a \geqslant b$).

Dividing equation (12) by (11) gives

$$\frac{\gamma_y}{\gamma_x} \equiv \delta = \frac{(1-k^2)^{-1}E(k) - K(k)}{K(k) - E(k)} \tag{13}$$

This means that if we know the axial ratio γ_y/γ_x of the confining potential V, equation (5), we can find the axial ratio a/b of the electron cloud. An example is shown in figure 1 [24, 25]. In fact, equation (13) demonstrates that the shapes are uniquely related *independent* of the number of electrons in the QD. Furthermore, the eccentricities of the external potential $V(x,y)$ and of the electron cloud it confines, $n(x,y)$, are not the same. This is highlighted in figure 2(a).

Once the eccentricity k of the pool of electrons is found, the spatial dimension a of the latter can then be obtained from

[3] One has to be careful about conflicts in notation found in reference books and computational packages. The present usage of K and E follows that found, for example, in [23]. AQ3

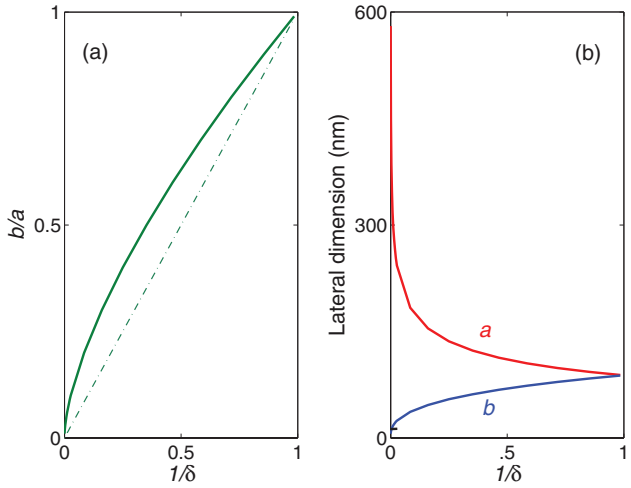

Figure 2. (a) The inverse axial ratio b/a of the electron droplet (solid line) in a quantum dot as a function of its confining potential's asymmetry δ, as determined by the universal relation (13). The shape of the cloud deviates from that of the potential well (dashed line). (b) The resulting semi-minor and semi-major axes of the electron droplet for the quantum dot described in figure 1. The limit of $\delta \to 1$ corresponds to a circular quantum dot, and $\delta \to \infty$ to the 1D limit. Note, however, that the calculation holds for axis lengths $\gg a_B^*$, equation (1). In the present example this point is reached at $\delta \sim 200$, as marked by a black dash.

equation (11) (and b follows from a and k). An example is illustrated in figure 2(b).

Directly from equations (10)–(12) we find the relation

$$\mu = \gamma_x a^2 + \gamma_y b^2. \tag{14}$$

In the round-dot limit, $\gamma_x = \gamma_y = \gamma$ and $a = b = R$, the above equation shows that the chemical potential becomes $\mu = 2\gamma R^2$ and together with equation (10) and the fact that $K(0) = \pi/2$ this reduces to the correct solution [14]

$$R^3 = \frac{3\pi}{8}\frac{Ne^{*2}}{\gamma}. \tag{15}$$

3.2. Electron energy

Now we can also calculate the total internal energy E_p of the dot's electrons which is composed of their mutual repulsion E_{ee} and the interaction with the external potential E_V. Recall that in the present approximation the kinetic energy of the electrons can be neglected. Thus $E_p = E_{ee} + E_V$, or

$$\begin{aligned} E_p &= \iint \left[\tfrac{1}{2}e\varphi(x,y) + V(x,y)\right] n(x,y)\mathrm{d}x\mathrm{d}y \\ &= \frac{1}{2}\iint [\mu + V(x,y)] n(x,y)\mathrm{d}x\mathrm{d}y \\ &= \frac{1}{2}\mu N + \frac{1}{2}\iint V(x,y) n(x,y)\mathrm{d}x\mathrm{d}y. \end{aligned} \tag{16}$$

where we made use of equation (3) in the second step and of the density normalization in the last step.

The results can be cast into several representations. An effective approach is to take advantage of a relation derived in the Appendix using a variational argument:

$$E_{ee} = 2E_V. \tag{17}$$

Together with the last line of equation (16) it is easily seen to result in

$$E_p = \frac{3}{5}\mu N. \tag{18}$$

One also can calculate the integral for E_V directly by substituting the potential from equation (5), the electron density from equation (7), and changing the variables to generalized polar coordinates ($x = ar\cos\theta$, $y = br\sin\theta$). Then one recovers precisely the relation (14).

And alternatively, if one wishes to express the answer only in terms of the confining potential parameters and the dot's eccentricities, so as to bring out the dominant N and shape dependences, one can use equations (18) together with equation (10), and in the latter expression use equation (11) to substitute for a in terms of γ_x. The result can be written

$$E_p = \frac{3}{5}\left(\frac{3}{2}\right)^{2/3} N^{5/3} e^{*4/3} \gamma_x^{1/3} \frac{k^{2/3}K(k)}{[K(k) - E(k)]^{1/3}}. \tag{19}$$

In the round-dot limit

$$E_p = \frac{3^{5/3}\pi^{2/3}}{10} N^{5/3} e^{*4/3} \gamma^{1/3}, \tag{20}$$

which can also be written in terms of the total electron charge $Q = Ne$ as

$$E_p = \frac{9\pi}{20}\frac{Q^2}{\varepsilon R}. \tag{21}$$

The variation of the quantum dot energy with the number of electrons N and with the deformation parameter is illustrated in figures 3(a) and (b). We see that deformation decreases the total internal energy of the quantum dot. (In a manner of speaking, this resembles the quantum-mechanical Jahn–Teller effect which favors oblate and prolate deformations for many nuclei and metal nanoclusters [7, 26, 27].)

This doesn't of course really imply that the minimal energy corresponds to extreme distortion (transformation into an almost 1D nanowire). Indeed, as marked in figure 2(b), the underlying approximation, that the electron droplet dimension is much greater than a_B^* and the kinetic energy is relatively small, breaks down when elliptical deformations become too large.

Nanostructure fabrication has enabled the formation not only of single QD electron pools within sandwiched semiconductor layers, but also of multiple barrier-separated electron puddles [28, 29]. The latter are also referred to as QD molecules [30]. Interestingly, the $N^{5/3}$ energy scaling suggests that distributing N electrons over n identical dots decreases the total electronic energy by a factor of $n^{2/3}$, potentially enhancing the stability of the system.

3.3. Quantum dot capacitance

The chemical potential of a QD with N electrons is the difference in total energy between two dots with same deformations containing N and $N-1$ electrons respectively,

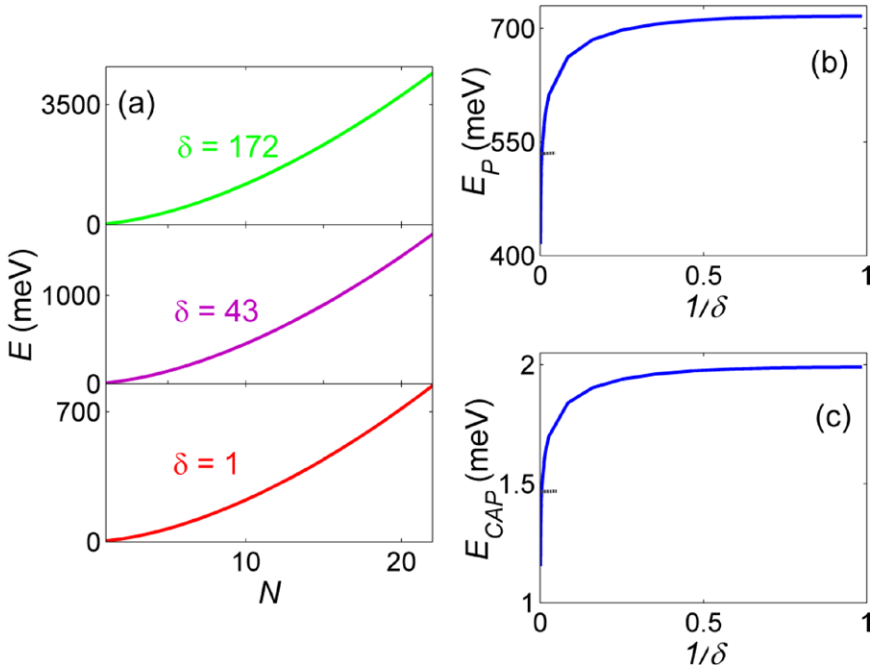

Figure 3. (a) Energy E_p of the electron system in elliptical quantum dots versus the number of confined electrons, for several values of the deformation parameter $\delta = \gamma_y/\gamma_x$ of the external potential V. (b) E_p versus the potential deformation parameter δ for a dot with $N = 20$ electrons. (c) Variation of the capacitive, or addition, energy, equation (23), with the deformation parameter δ for $N = 20$. The examples are for InGaAs, as in figure 1. Black dashes correspond to the same limit of applicability as in figure 2.

$$\mu(N) = E_p(N) - E_p(N-1). \tag{22}$$

The electron addition energy, also known as the capacitive energy, is [31, 32]

$$\frac{e^{*2}}{C(N)} = \mu(N+1) - \mu(N), \tag{23}$$

i.e. the second difference $E_p\,(N+1) + E_p\,(N-1) - 2E_p\,(N)$.

The variation of the capacitive energy with the degree of dot deformation δ for a fixed number of electrons N is illustrated in figure 3(c). This quantity is of particular interest from the experimental point of view. For example, it has been measured in circular QD in [1] and in rectangular QD with rounded corners (i.e. close to elliptical) in [3]. Figure 4 shows the experimental data and numerical density function theory (DFT) calculations together with our results for the same parameters. Clearly, the present analytical results describe the size and shape variation of the capacitive energies extremely well.

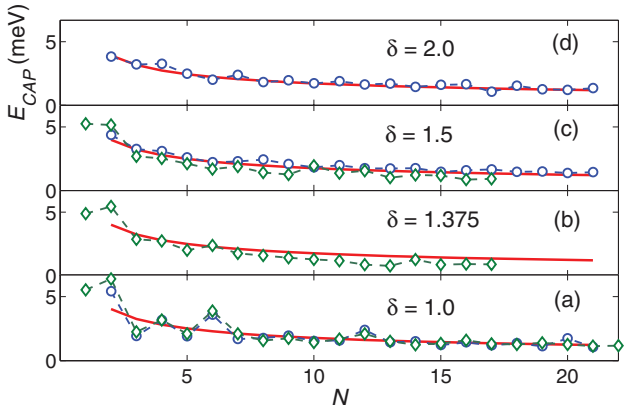

Figure 4. A comparison of capacitive (electron addition) energies derived in this work with experimental and numerical results for elliptical InGaAs (as in figure 1) quantum dots, for different degrees of deformation of the confining potential. Green diamonds: experimental data on circular [1] and rectangular [3] QD. Blue circles: local spin-density approximation (LSDA) calculation [3, 24] taking the curvature of the confining potential to be $\gamma = e^{*2}/(2r_0^3 N^{1/2})$, $r_0 = 1.5a_B^*$, and approximating rectangular dots with rounded-off corners as ellipses with the axial ratio δ of the latter equal to the edge length ratio of the former. (The peaks in the data at $N = 2$, 6, 12 are due to quantum 2D shell closings.) Solid red line: values obtained from the analytical energy expression in the text, equation (23), calculated using the same parameters.

4. 3D ellipsoidal quantum dots

4.1. Electron distribution

The treatment of an electron droplet confined within a 3D harmonic potential

$$V(\vec{r}) = \gamma_x x^2 + \gamma_y y^2 + \gamma_z z^2 \tag{24}$$

to a large degree parallels the 2D case considered above.

However, there is a significant difference in how the electrons distribute themselves within the dot. Within the electrostatic approximation (applicable, as above, when the electron distribution is not varying rapidly and its size is much larger than the effective Bohr radius a_B^*) the density of electrons in the 3D case is constant throughout the QD, as opposed to peaking near the origin as in 2D, equation (7). Indeed, the electrons will distribute themselves so as to create a potential balancing out $V(\vec{r})$, and it well known [33–35] that a uniformly charged dielectric ellipsoid creates a quadratic potential

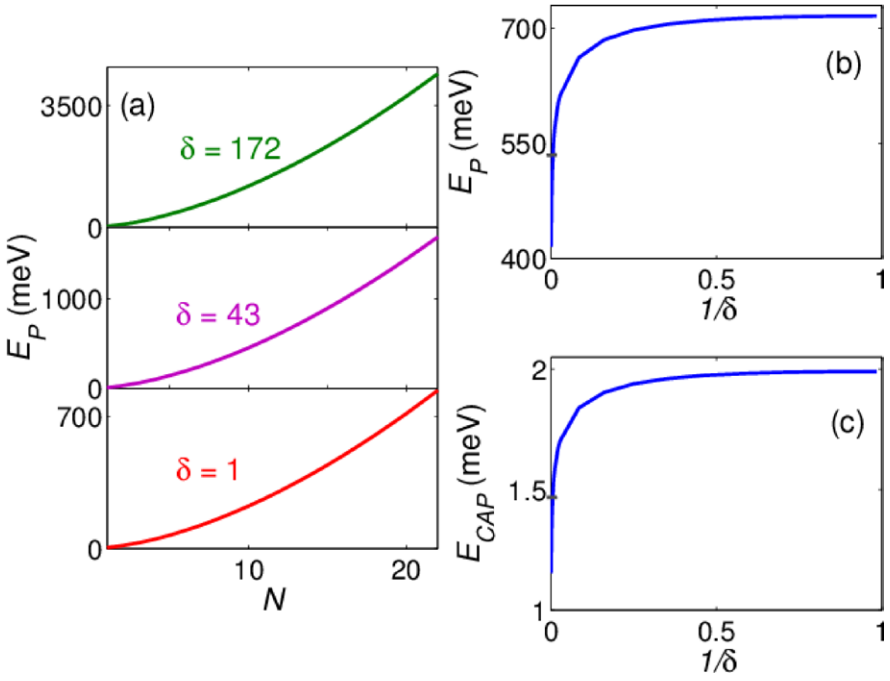

Figure 5. (a) Electron droplet inverse axial ratio for an oblate spheroid ($\gamma_x = \gamma_y < \gamma_z$, $a = b > c$) as a function of the confining potential well's deformation parameter $\delta = \gamma_z/\gamma_x$, as determined by the universal relation (28). The shape of the droplet deviates from that of the potential well (dashed line). (b) The resulting semi-minor and semi-major axes of the electron cloud for an $In_{0.05}Ga_{0.95}As$ dot ($\varepsilon = 12.9$, $m^* = 0.067$) with $N = 100$ electrons and the confinement force constant $\gamma = 3.95$ μeV nm^{-2}. The calculation holds for axis lengths $\gg a_B^*$, equation (1). In the present example this point is reached at $\delta \sim 25$, as marked by a dash.

$$\varphi(\vec{r}) = \frac{2\pi en}{\varepsilon}(A - D_x x^2 - D_y y^2 - D_z z^2) \tag{25}$$

Here

$$n = \frac{3}{4\pi}\frac{N}{abc} \tag{26}$$

is the electron number density (N is the total number of electrons in the QD) and D_i are the familiar tabulated [34, 35] depolarization factors. If the ellipsoidal charge distribution has semi-axes $\{a,b,c\}$ they're given by

$$D_i = \frac{abc}{2}\int_0^\infty \frac{\mathrm{d}\xi}{(\nu_i^2+\xi)\sqrt{(a^2+\xi)(b^2+\xi)(c^2+\xi)}} \tag{27}$$

(with $\nu_i = \{a,b,c\}$ for $i = \{x,y,z\}$, respectively) and are expressible in terms of elliptic integrals. It is assumed that we choose $a \geqslant b \geqslant c \geqslant 0$.

The electron–electron repulsion, equation (25), will precisely balance the potential V, equation (24), so obviously the shape of the electron droplet is determined by setting

$$\gamma_i = \frac{3Ne^{*2}}{2abc}D_i(\varphi,\theta) \tag{28}$$

and solving for the unknowns $\{a,b,c\}$ in terms of $\{\gamma_x,\gamma_y,\gamma_z\}$. Here [34] $\cos\varphi = b/a$ and $\cos\theta = c/a$. Again, we see that the shapes of the electron droplet and the confinement potential are related to each other purely in terms of their axial ratios, independent of the number of electrons.

As in the 2D case, the shape of the electron droplet will be different from that of the confining potential. (This is simply a restatement of the fact that the harmonic potential (25) has a different shape than the uniform charged ellipsoid which gives rise to this potential.) Figure 5 illustrates the result for the case of spheroidal confinement (when the depolarization factors can be expressed in terms of elementary functions [34–36]).

In the round-dot limit $\gamma_x = \gamma_y = \gamma_z = \gamma$ and $a = b = c = R$, and with the depolarization factors of a sphere equal to 1/3, equation (28) reduces to the result which follows from the potential of a uniformly charged sphere:

$$R^3 = \frac{Ne^{*2}}{2\gamma}, \tag{29}$$

differing from the 2D solution (15) only by a numerical factor.

The chemical potential, as follows from equations (3), (25) and (26) and the expression for A given in [33], is

$$\mu = \frac{3}{2}\frac{Ne^{*2}}{\sqrt{a^2-c^2}}F(k,\theta), \tag{30}$$

where F is the elliptic integral of the first kind, $k = \sqrt{(a^2-b^2)/(a^2-c^2)} = \sin\varphi/\sin\theta$ and the angles θ and φ are defined above.

4.2. Quantum dot energy and capacitance

The total energy of the 3D dot's electrons, $E_p = E_{ee} + E_V$, is calculated in the same way as in the 2D case of section 3.2. The variational condition (17) and its corollary (18) hold in the present case as well.

Direct evaluation of the integral for E_V, as in equation (16), in the present case of uniform electron density, equation (26), can be performed using generalized spherical coordinates

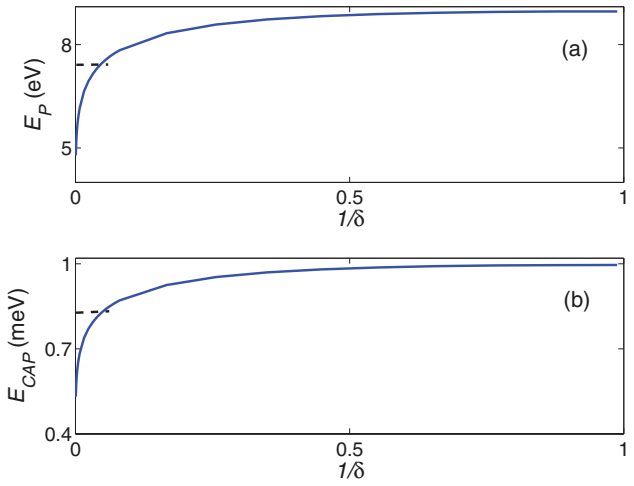

Figure 6. (a) The total internal energy, E_p, for an oblate 3D $In_{0.05}Ga_{0.95}As$ dot with the same parameters as figure 5(b), as a function of the confinement deformation parameter $\delta = \gamma_z/\gamma_x$. (b) Variation of the dot's capacitive energy with δ.

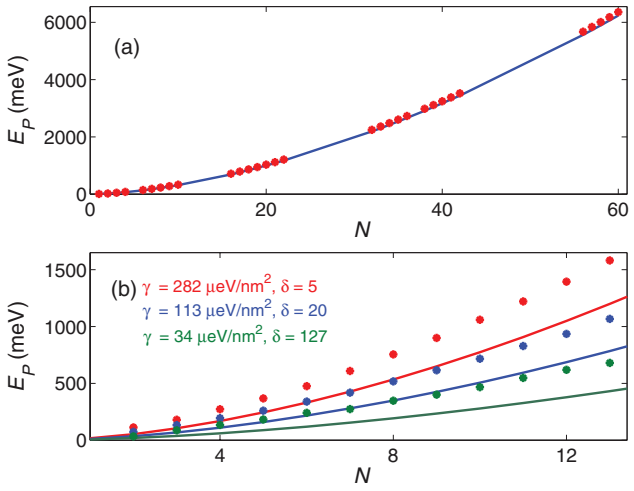

Figure 7. (a) The internal energy of a spherically symmetric 3D quantum dot confined in GaAs. Dots: computation by the relativistic coupled cluster method [37] for $\varepsilon = 12.4$, $m^* = 0.067$, confinement strength $\gamma = 15.8$ μeV nm^{-2}), line: present analytical results using the same parameters. (b) The electron energy of oblate spheroidal GaAs QD. Circles: spin DFT calculations [38] for three different confinement strengths, lines: present results using the same parameters.

$(x = ar\cos\varphi\sin\theta, \quad y = br\sin\varphi\sin\theta, \quad z = cr\cos\theta, \quad$ Jacobian $J = abcr^2\sin\theta)$. Then precisely the same form as the 2D case (14) follows: $\mu = \gamma_x a^2 + \gamma_y b^2 + \gamma_z z^2$.

Figure 6(a) illustrates the shape dependence of the 3D QD energy for the case of spheroidal ($\gamma_x = \gamma_y$) confinement. Here it is convenient again to use a deformation parameter δ to write $\gamma_x = \gamma_y = \delta^{-1/3}\gamma$, $\gamma_z = \delta^{2/3}\gamma$.

For an isotropic QD the total energy reduces to the value corresponding to a uniformly charged sphere

$$E_p = \frac{9}{10}\frac{(Ne)^2}{\varepsilon R} = \frac{9}{5\cdot 2^{2/3}} N^{5/3} e^{*4/3}\gamma^{1/3} \tag{31}$$

This differs from the expression (20) for a 2D dot with the same number of electrons and external potential curvature by a factor of $(6/\pi^2)^{1/3}$.

Figure 7(a) compares the above expression for a symmetric 3D dot with the values obtained in [37] by the coupled-cluster method. The present analytical model provides an excellent match with the numerically intensive calculation.

In figure 7(b) the results for a nonspherical QD are compared with the density-functional computation in [38]. Here, as the confining potential along the vertical axis is kept unchanged and that in the horizontal plane is gradually relaxed, the total internal energy of the system decreases, as expected: in a flatter external potential well the electron cloud spreads out over a larger volume. The calculated trends are very similar, although there is a mismatch in the absolute magnitude. Interestingly, as pointed out below, the energy *differences* are in very good agreement. It would be useful to replicate the DFT results and to investigate if they contain a possible energy offset.

The QD capacitive, or addition, energy is defined as above, equation (23). An example of its shape dependence for a spheroidal system is illustrated in figure 6(b). The size variation of this quantity is compared with Hartree–Fock calculations for a spherical dot [39] and with DFT calculations for a spheroidal dot [38] in figure 7. Apart from quantum shell oscillations, which cannot be reproduced by (semi)classical methods, the analytical theory demonstrates excellent agreement, with no adjustable parameters.

5. Summary

The properties of a multielectron system, such as a quantum dot, can be represented as quantum oscillations around a smooth evolution with size. In this paper we obtain fully analytical expressions for the average size-dependent quantities (electron droplet dimension, shape, and density, the total energy, the chemical potential, and the capacitive energy) for carriers confined within 2D elliptical and 3D ellipsoidal quantum dots by a harmonic external potential.

Such confinement geometry corresponds to the most commonly implemented practical situations, and the analytical solution makes it possible to follow the variation of important quantities over a wide range of parameters (such as the total number of electrons, the axial ratios and curvatures of the confinement potential, and the dielectric constant of the material). The results obtained are in very good agreement with the published experimental data and numerically computed values.

The solution is facilitated by the rigorously established fact that for a sufficiently large size of the confined electron droplet (specifically, when its size is much larger than the effective Bohr radius a_B^*, equation (1)) the dominant contribution to the Thomas–Fermi problem of confinement equilibrium comes from the potential energy terms. As a result, the case of 2D confinement is aided by the electrostatic analogue of the Hertz elastic contact problem, and that of 3D confinement is expressed with the help of depolarization factors. One also can derive a useful relation between the electrostatic and external potential energies, equation (17), using a variational approach.

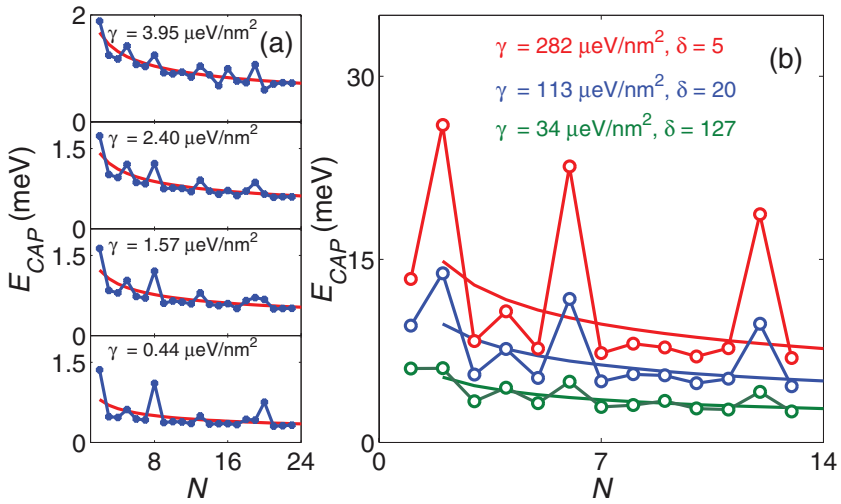

Figure 8. (a) Capacitive (electron addition) energy for a spherically symmetric GaAs quantum dot for different strength of confining potential. Circles: Hartree–Fock calculation [39]; lines: present analytical results for the same parameters. (b) Capacitive energies for oblate quantum dots. Circles: spin DFT calculations [38]; lines: present results. (Peaks are assigned to quantum shell closings). AQ5

One interesting feature of the solution, possibly unintuitive at the outset, is that the eccentricity (i.e. the axial ratios) of the electron droplet, in both the 2D and 3D cases, is not the same as that of its external confinement potential. The relationship between the two is derived and is shown to depend only on the shape of the potential well (the ratios of its axial force constants) and not on the number of the electrons, the size of the dot, or any other parameters.

The approach can be extended to study the effect of point impurities introduced inside the quantum dots, as well as the perturbative effects of anharmonicities in the confinement potential. These problems will be considered elsewhere. Newly developed families of 2D semiconductors [40] such as silicene, phosphorene, and germanene represent another potential stage for applications of the theory.

Acknowledgments

This research was supported by the U.S. National Science Foundation under Grant No. DMR-1206334. A.H. acknowledges the support by the U.S. Department of Energy (DOE), Office of Science, Basic Energy Sciences, Division of Materials Sciences and Engineering under Contract No. AQ4 DE-AC-02-06CH11357.

Appendix

Equation (17) can be derived using a scaling variational method. We follow [41] where the same method is applied to derive the virial theorem for the Thomas–Fermi model of the atom. We replace $n(x,y)$ by the set of functions $n_\lambda(x,y) = \lambda^2 n(\lambda x,\lambda y)$ which all satisfy the normalization condition $\int n_\lambda(x,y)\mathrm{d}x\mathrm{d}y = N$. The constituents of the total energy then transform as $E_{ee}(\lambda) = \lambda E_{ee}$ and $E_V(\lambda) = \lambda^{-2}E_V$ so that $E_p(\lambda) = \lambda E_{ee} + \lambda^{-2}E_V$. In the equilibrium configuration the energy is minimized, i.e. $\partial E_p(\lambda)/\partial\lambda = 0$ for $\lambda = 1$. This immediately leads to equation (17).

References AQ6

[1] Kouwenhoven L P, Austing D G and Tarucha S 2001 *Rep. Prog. Phys.* **64** 701
[2] Drexler H, Leonard D, Hansen W, Kotthaus J P and Petroff P M 1994 *Phys. Rev. Lett.* **73** 2252
[3] Austing D G, Sasaki S, Tarucha S, Reimann S M, Koskinen M and Manninen M 1999 *Phys. Rev.* B **60** 11514
[4] Meurer B, Heitmann D and Ploog K 1993 *Phys. Rev.* B **48** 11488
[5] Brack M 1993 *Rev. Mod. Phys.* **65** 677
[6] Kresin V V 1992 *Phys. Rep.* **220** 1
[7] Nilsson S G and Ragnarsson I 1995 *Shapes and Shells in Nuclear Structure* (Cambridge: Cambridge University Press)
[8] Yannouleas C and Landman U 1993 *Phys. Rev.* B **48** 8376
[9] 1983 *Theory of the Inhomogeneous Electron Gas* ed S Lundqvist and N H March (New York: Plenum) AQ7
[10] Lieb E H 1981 *Rev. Mod. Phys.* **53** 603
Lieb E H 1982 *Rev. Mod. Phys.* **54** 311
[11] Englert B-G 1988 *Semiclassical Theory of Atoms* (Berlin: Springer)
[12] Brack M and Bhaduri R K 2003 *Semiclassical Physics* (Boulder: Westview)
[13] Räsänen E, Pittalis S, Bekçioğlu G and Makkonen I 2013 *Phys. Rev.* B **87** 035144
[14] Shikin V, Nazin S, Heitmann D and Demel T 1991 *Phys. Rev.* B **43** 11903
[15] Ovchinnikov Y N, Halder A and Kresin V V 2014 *Europhys. Lett.* **107** 37001
[16] García-Moliner F and Flores F 1979 *Introduction to the Theory of Solid Surfaces* (Cambridge: Cambridge University Press) section 3.2
[17] Odriazola A, Gonzales A and Räsänen E 2014 *J. Phys.: Condens. Matter* **26** 355501
[18] Sañudo J and Pacheco A F 2008 *Int. J. Mod. Phys.* B **22** 469
[19] Landau L D and Lifshitz E M 1970 *Theory of Elasticity* 2nd edn (Oxford: Pergamon) section 9
[20] Shikin V B and Leiderer P 1983 *Solid State Commun.* **47** 269
[21] Shikin V B 1984 *Sov. Phys. JETP* **59** 304
[22] Johnson K L 1985 *Contact Mechanics* (Cambridge: Cambridge University Press) ch 3
[23] Gradshteyn I S and Ryzhik I M 2007 *Table of Integrals, Series, and Products* 5th edn (Burlington: Academic)
[24] Ezaki T, Mori N and Hamaguchi C 1997 *Phys. Rev.* B **56** 6428

[25] Tarucha S, Austing D G, Honda T, van der Hage R J and Kouwenhoven L P 1996 *Phys. Rev. Lett.* **77** 3613
[26] Clemenger K 1985 *Phys. Rev.* B **32** 1359
[27] de Heer W A 1993 *Rev. Mod. Phys.* **65** 611
[28] Heitmann D and Kotthaus J P 1993 *Phys. Today* **46** 56
[29] Brodsky M, Zhitenev N B, Ashoori R C, Pfeiffer L N and West K W 2000 *Phys. Rev. Lett.* **85** 2356
[30] Reimann S and Manninen M 2002 *Rev. Mod. Phys.* **74** 1283
[31] Kastner M A 1993 *Phys. Today* **46** 24
[32] Iafrate G J, Hess K, Krieger J B and Macucci M 1995 *Phys. Rev.* B **52** 10737
[33] Kellogg O D 1967 *Foundations of Potential Theory* (Berlin: Springer) (reprint of the 1929 edition) ch VII
[34] Osborn J A 1945 *Phys. Rev.* **67** 351
[35] Stoner E C 1945 *Phil. Mag.* **36** 803
[36] Landau L D, Lifshitz E M and Pitaevskii L P 1984 *Electrodynamics of Continuous Media* 2nd edn (Oxford: Pergamon)
[37] Yakobi H, Eliav E and Kaldor U 2011 *J. Chem. Phys.* **134** 054503
[38] Lee I-H, Rao V, Martin R M and Leburton J-P 1998 *Phys. Rev.* B **57** 9035
[39] Vorrath T and Blümel R 2003 *Eur. Phys. J.* B **32** 227
[40] Bhimanapati G R *et al* 2015 *ACS Nano* **9** 11509
[41] Flügge S 1971 *Practical Quantum Mechanics* (Berlin: Springer) section IVB

QUERIES

Page 1
AQ1
Please specify the corresponding author and provide his/her email address.
AQ2
Please be aware that the colour figures in this article will only appear in colour in the online version. If you require colour in the printed journal and have not previously arranged it, please contact the Production Editor now.
Page 3
AQ3
Text from the reference [23] has been moved and set as a footnote in the text as required by our style. Please check and confirm that it has been inserted correctly within the text.
Page 8
AQ4
We have been provided funding information for this article as below. Please confirm whether this information is correct.
"1. Division of Materials Research: DMR1206334; 2. Argonne National Laboratory, Office of Science: DE-AC-02-06CH11357".
AQ5
Figure 8 is not cited in text but has been provided. Please remove figure or provide citation.
AQ6
Please check the details for any journal references that do not have a link as they may contain some incorrect information.
AQ7
Please provide author names or collaboration name for reference [9].